Rapid Communications

Low-temperature specific heat of doped $SrTiO_3$: Doping dependence of the effective mass and Kadowaki-Woods scaling violation

E. McCalla,[1,2] M. N. Gastiasoro,[3] G. Cassuto,[1] R. M. Fernandes,[3] and C. Leighton[1,*]

[1]*Department of Chemical Engineering and Materials Science, University of Minnesota, Minneapolis, Minnesota 55455, USA*

[2]*Department of Chemistry, McGill University, Montreal, Canada*

[3]*School of Physics and Astronomy, University of Minnesota, Minneapolis, Minnesota 55455, USA*

(Received 13 August 2018; published 15 February 2019)

We report wide-doping-range (8×10^{17} to 4×10^{20} cm^{-3} Hall electron density) low-temperature specific heat measurements on single crystal $SrTiO_3$:Nb, correlated with electronic transport data and tight-binding modeling. Lattice dynamic contributions to specific heat are shown to be well understood, albeit with unusual sensitivity to doping, likely related to the behavior of soft modes. Electronic contributions to specific heat provide effective masses that increase substantially, from 1.8 to $4.8m_e$, across the two $SrTiO_3$ Lifshitz transitions. It is shown that this behavior can be quantitatively reconciled with quantum oscillation data and calculated band structure, establishing a remarkably doping-independent mass enhancement factor of 2.0. Most importantly, with the doping-dependent T^2 resistivity prefactor and Sommerfeld coefficient known, Kadowaki-Woods scaling has been tested over the entire doping range probed. Despite classic Fermi liquid behavior in electronic specific heat, standard Kadowaki-Woods scaling is dramatically violated, highlighting the need for new theoretical descriptions of T^2 resistivity in $SrTiO_3$.

DOI: 10.1103/PhysRevMaterials.3.022001

Few materials have posed such challenges to condensed-matter physics as the perovskite oxide $SrTiO_3$. From the structural and lattice dynamic perspective, this material has revealed an extraordinary low-temperature (T) quantum paraelectric state where ferroelectricity is suppressed by quantum fluctuations [1–5], in addition to a second-order antiferrodisplacive structural transformation at 105 K [5–9]. The former is associated with $T \to 0$ softening of a zero wave-vector transverse phonon [1–5], whereas the latter is related to softening of a zone-boundary octahedral rotation mode [5–9]. Quantum paraelectricity also leads to interesting physics when $SrTiO_3$ is doped. n-doping with Nb^{5+} and La^{3+} (for Ti^{4+} and Sr^{2+}) has been explored, along with oxygen vacancy doping [10–14]. Due to the high dielectric constant (>10 000 at low T [1,3,4]), donors in $SrTiO_3$ have unusually large Bohr radii (~600 nm), vanishing ionization energies, and highly screened ionized scattering potentials [10–14]. Donor wave functions thus overlap at very low electron density (n), generating a remarkable low-density high-mobility metallic state [10–14]. Metallic transport has been claimed to $n < 10^{16}$ cm^{-3} [14] in fact, with a well-defined Fermi surface down to ~10^{17} cm^{-3} [15,16].

The very small Fermi surface of this dilute metal has been studied by Shubnikov–de Haas (SdH) oscillations [15–18], angle-resolved photoemission spectroscopy (ARPES) [19], and density functional theory (DFT) [20–22]. In the low-T tetragonal state, the Ti^{4+} t_{2g} states at the conduction-band minimum are split by tetragonality (by ~2–5 meV) and spin-orbit interactions (by ~12–30 meV) [15–22]. Two Lifshitz transitions thus occur vs n in $SrTiO_3$, corresponding to first occupation of the tetragonality-split band (at $n_{c1} \approx 1.5 \times 10^{18}$ cm^{-3}) and the spin-orbit-split band (at $n_{c2} \approx 2 \times 10^{19}$ cm^{-3}) [15–22]. The three bands have varying anisotropies and dispersions, leading to effective mass (m^*) that varies from ~$1.5m_e$ (m_e is the free-electron mass) to 4–$6m_e$ as the Lifshitz transitions are crossed [16]. While the agreement on band splittings and masses among SdH measurements, between SdH and ARPES, and between experiment and theory is generally reasonable, significant uncertainties remain, particularly at high n.

Superconductivity leads to further interest in $SrTiO_3$. This was, in fact, the first oxide superconductor discovered, the first semiconductor known to superconduct, and the first example of a superconducting "dome" [11,23]. Superconductivity also occurs to extraordinarily low n (3×10^{17} cm^{-3}), with subtle interplay with band filling [16,24], leading to several proposals for novel pairing mechanisms [25–29]. Recently, normal-state transport in doped $SrTiO_3$ has also come under intense scrutiny [21,30–34]. In particular, below 60–100 K, $SrTiO_3$ has been found to exhibit the T^2 resistivity (ρ) often taken as evidence of Fermi liquid behavior [21,30–34]. This is a puzzling observation, however. At $n < n_{c1}$, for example, the tiny Fermi surface, low Fermi temperature, and single filled electron reservoir appear to rule out the scattering processes (e.g., umklapp) typically needed to generate resistivity of the form $\rho \propto \rho_0 + AT^2$ [32]. The electron scattering rate is also independent of n over four orders of magnitude (or, equivalently, $A \propto 1/n$), which has been stated to be at odds with theory [33,34]. These observations, among others, have raised doubts over the Fermi liquid nature of the metallic state in this foundational oxide.

*Corresponding author: leighton@umn.edu

In principle, heat capacity (C_P) measurements have the potential to greatly elucidate much of the above. Lattice dynamic contributions to C_P, for example, could probe the complex low-T evolution of phonon modes in $SrTiO_3$. Unfortunately, even basic parameters such as the Debye temperature θ_D are remarkably scattered in the $SrTiO_3$ literature, as discussed in the Supplemental Material, Sec. A (Table SI) [35] [30,31,36–42]. Moreover, electronic contributions to C_P could probe the following: the existence of a well-defined γT contribution (where γ is the Sommerfeld coefficient), as expected in a Fermi liquid; the density-of-states effective mass (m^*_{DOS}) vs n (for comparison to SdH, DFT, etc.); and Kadowaki-Woods scaling. The latter refers to the well-known linear scaling between A and γ^2 that is empirically established in Fermi liquids such as transition metals and heavy fermion compounds [43,44]. Again, however, the literature on $\gamma(n)$ [and thus $m^*_{DOS}(n)$] in $SrTiO_3$ is highly inconsistent, as shown in the Supplemental Material, Sec. A, Fig. S1 [35]. The use of polycrystalline [36–38,41] and potentially inhomogeneous [36,41] samples, impurity-related Schottky anomalies [38,39], and the limited doping ranges studied [30,31,36–42] all likely contribute to this inconsistency. Intriguingly, however, while the number of data points is very limited, the existing data on A and γ do indicate potential violation of Kadowaki-Woods scaling in La-doped $SrTiO_3$ [30,31].

Here, we rectify this situation through a wide-n-range (8×10^{17} to 4×10^{20} cm^{-3}) low-temperature $C_P(T)$ study of thoroughly characterized $SrTiO_3$:Nb single crystals, correlated with $\rho(T)$ measurements and tight-binding modeling. It is shown that lattice dynamic contributions to C_P can be understood, albeit with unusual sensitivity to doping, potentially related to incipient ferroelectricity. A well-defined Fermi-liquid-like γT contribution to C_P is then isolated, supported by theory, providing detailed $\gamma(n)$ data for comparison to $A(n)$. The n dependence of m^*_{DOS} is thus significantly clarified, and reconciled with SdH measurements and band structure calculations, establishing a completely *n-independent* mass enhancement factor of 2.0. Most importantly, despite the Fermi-liquid-like electronic C_P, A is found to *decrease* by two orders of magnitude with increasing γ, leading to striking violation of standard Kadowaki-Woods scaling, with deep implications for the origin of the T^2 resistivity.

The Nb-doped single crystals studied here are some of the same ones used in prior work, and have been characterized by x-ray diffraction [14], impurity analysis [45], and resistivity, Hall effect, mobility (μ), and magnetoresistance measurements [14]. Nb content (x in $SrTi_{1-x}Nb_xO_3$), n(300 K), ρ(300 K), and μ(4 K) are shown in Table SII of the Supplemental Material, Sec. B [35], which also includes a discussion of methods. Briefly, short-pulse relaxation calorimetry was used, with great attention paid to errors associated with thermal coupling and sample-to-addenda C_P ratios [46]. Figure 1(a) first shows wide-T-range $C_P(T)$ for these crystals. Aside from small anomalies around the structural transformation at 105–130 K (with doping dependence studied in prior work [9]), $C_P(T)$ is qualitatively as expected, with only minor apparent x dependence. Figure 1(b) shows typical analysis of low-T data (1.8 to 9 K), where C_P/T is plotted vs T^2 to test the relation $C_P(T) = \beta T^3 + \gamma T$. Here, βT^3 is the Debye lattice term (where $\beta = 234 N k_B/\theta_D^3$, N is the number of ions/mole, and k_B is Boltzmann's constant), and γT captures electronic contributions. In a single-band free-electron model, $\gamma = m^*_{DOS}\, n^{1/3} (k_B/\hbar)^2 (\pi/3)^{2/3}$, where $\hbar = h/2\pi$ and h is Planck's constant. As illustrated by the solid line fits

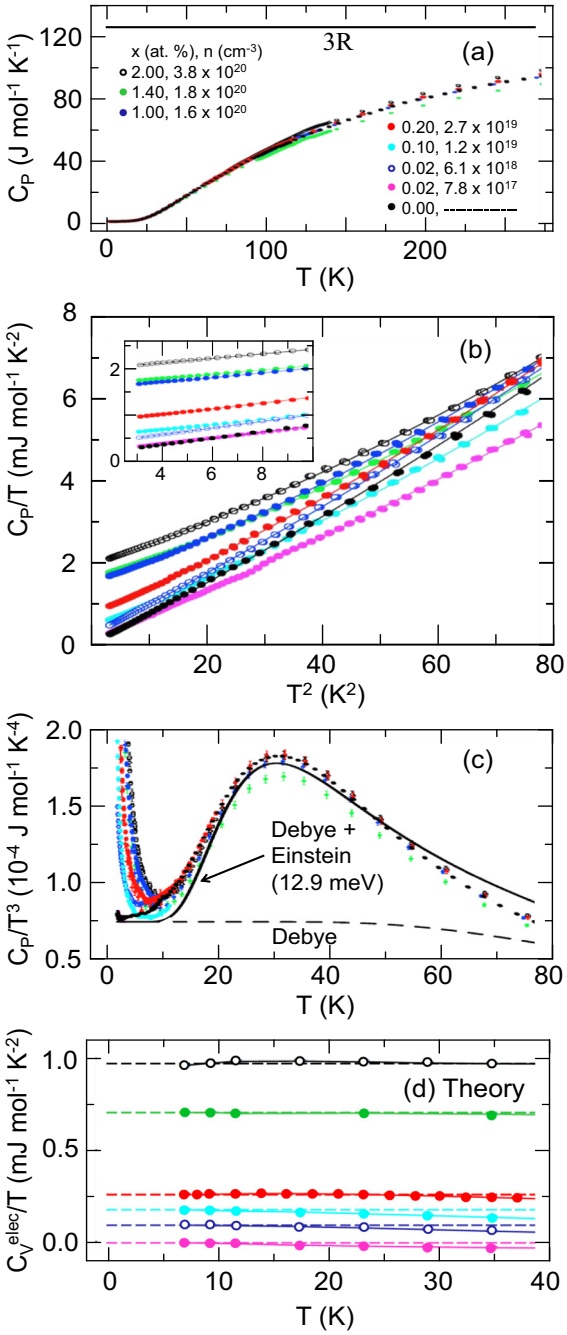

FIG. 1. (a) Specific heat (C_P) vs temperature (T) from 1.8–280 K, with Nb contents (x) and Hall densities (n) labeled. The horizontal line marks the Dulong-Petit value. (b) C_P/T vs T^2 up to ~9 K, with solid line fits discussed in the text. Inset: Expanded view from 1.8–3.2 K. (c) C_P/T^3 vs T up to 80 K. The dashed line shows Debye $C_P(T)$ for a Debye temperature of 560 K; the solid line fit adds the Einstein contribution discussed in the text. (d) *Theoretical* electronic heat capacity, plotted as C_V^{elec}/T vs T for the same n values studied experimentally. Horizontal dashed lines mark the Sommerfeld coefficient as $T \to 0$.

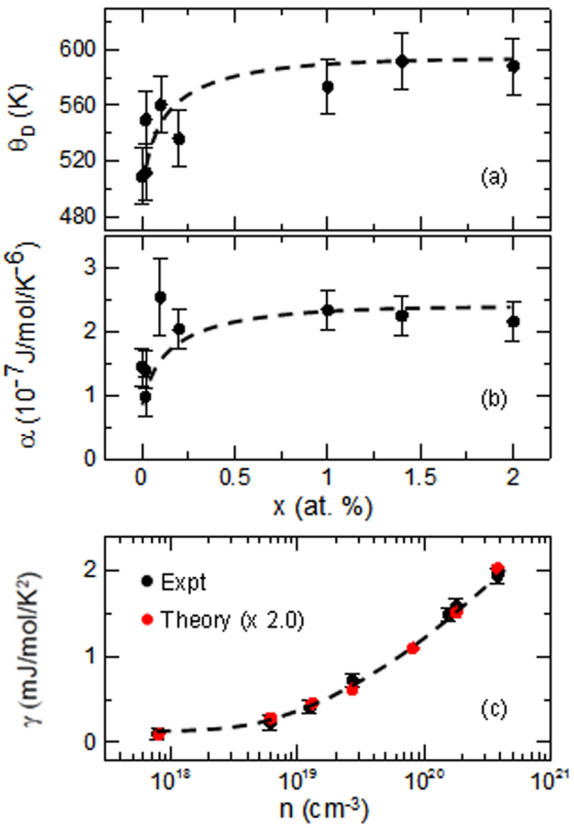

FIG. 2. Nb content (x) dependence of (a) the Debye temperature (θ_D) and (b) the T^5 specific-heat prefactor (α). (c) Hall electron density (n) dependence of the Sommerfeld coefficient (γ). Shown are experimental points, and theoretical values [from Fig. 1(d)] multiplied by 2.0. Dashed lines are guides to the eye.

in the inset to Fig. 1(b), this form describes the data very well up to 3–4 K, with an intercept γ that increases with n. As shown in the main panel, however, at higher T, up to 9 K, upward curvature is apparent in C_P/T vs T^2. As is often required, we thus add a next-order Debye term in $C_P(T) = \beta T^3 + \alpha T^5 + \gamma T$, resulting in the good fits shown in Fig. 1(b). The resulting θ_D, α, and γ are plotted in Fig. 2.

We discuss first the lattice dynamic contributions to $C_P(T)$, returning below to electronic contributions. While the undoped $SrTiO_3$ θ_D of 515 ± 20 K [Fig. 2(a)] is larger than many of the early, widely scattered values (see the Supplemental Material, Sec. A [35]), it is in excellent agreement with recent single crystal work [40]. Surprisingly, however, θ_D is sensitive to even light doping. As shown in Fig. 2(a), θ_D increases to 570–590 K at $x = 1\%$, where it plateaus. This increase is above uncertainty and is, in fact, readily apparent in Fig. 1(b), where the slope clearly decreases with doping. Interestingly, this increase in θ_D, and upward curvature in $C_P(T)$ vs T^2, were also noted by Ahrens *et al.* [40], who rejected the possibility of such sensitivity to doping and thefore fixed θ_D at its undoped value. In our case, θ_D is independent of whether fitting is performed over the range in the inset to Fig. 1(b), with no T^5 term, or the range in the main panel, with T^5 included. We thus have high confidence in the $\theta_D(x)$ in Fig. 2(a), whose behavior is mirrored in $\alpha(x)$ [Fig. 2(b)]. Note that in all cases, the αT^5 contribution to C_P is indeed substantially smaller than βT^3, as expected.

We contend that established trends in soft-mode frequencies in $SrTiO_3$ provide potential explanations for Figs. 2(a) and 2(b). It is known, for example, that the antiferrodisplacive transformation temperature shifts from 105 to 130 K in this x range [9], which could increase the low-T frequencies of the corresponding modes, thereby increasing θ_D. The transformation temperature shift is linear in x, however, which is difficult to reconcile with the sharp increase at low x seen in Figs. 2(a) and 2(b). Alternatively, the $T \to 0$ softening of the ferroelectric mode in $SrTiO_3$ should also weaken with doping (i.e., the frequency should increase) due to screening of interdipole interactions. This is analogous to the situation in $Sr_{1-x}Ca_xTiO_{3-\delta}$, where increased n suppresses the cubic-to-tetragonal "ferroelectric" transition [47]. Simple estimates indicate that taking into account the expected decrease in dielectric constant with doping, the Thomas-Fermi screening length could indeed approach the Ti-O-Ti distance at low n in $SrTiO_3$, potentially explaining Fig. 2(a).

A final interesting point on lattice dynamics is highlighted in Fig. 1(c), where C_P/T^3 is plotted vs T, to higher T than in Fig. 1(b). Such plots expose deviations from Debye behavior (dashed line), which are apparent in $SrTiO_3$ as a peak in excess C_p around 30 K. This is a known phenomeon in perovskite oxides, thought to occur due to excess lattice C_p associated with the first maximum in the phonon density of states [40,48]. The solid line in Fig. 1(c) is a fit to the Einstein expression, $C_P(T) = 3Rw(\theta_E/2T)^2 \sinh^{-2}(\theta_E/2T)$, where R is the gas constant, w is a weight factor, and θ_E is the Einstein temperature ($\hbar\omega_0/k_B$, where ω_0 is the phonon frequency). This describes the excess C_P well, with $\hbar\omega_0 = 12.9$ meV, in good agreement with prior work [40] and the first peak in the $SrTiO_3$ phonon density of states [49]. The peak in Fig. 1(c) is x independent in this range, as expected for these particular phonons, which are not soft modes.

We now turn to electronic contributions to $C_P(T)$. As noted above, analysis of Fig. 1(b) suggests that these may be captured with the standard γT Fermi liquid form. It is not, however, *a priori* clear that such analysis is even valid in this T range; the Fermi energy and temperature are as low as 1.7 meV and 16 K, and Fermi liquid behavior has been questioned. To inform our analysis, we thus used a tight-binding fit to the DFT-calculated structure of the conduction-band minimum in $SrTiO_3$ [21], as shown in Fig. 3(a). Shown here are the three t_{2g}-derived bands, the tetragonal and spin-orbit splittings, and the critical densities for the two Lifshitz transitions, n_{c1}, and n_{c2}. The electronic specific heat, $C_V^{elec}(T)$, was then computed from a self-consistent calculation of the chemical potential $\mu(T)$ and eigenstates $E_{ik}(T)$ of each band i, for a given n, using a $120 \times 120 \times 120$ three-dimensional k grid. $C_V^{elec}(T) = T\frac{\partial S}{\partial T}$ is then calculated from the entropy, $S(T) = -2k_B \sum_{ik}\{f(E_{ik})\ln[f(E_{ik})] + f(-E_{ik})\ln[f(-E_{ik})]\}$. The results are shown in Fig. 1(d), where C_V/T is plotted vs T. While deviations from linearity are present (compare the data to the horizontal dashed lines), particularly at low n, even at 7.8×10^{17} cm^{-3} these occur only above $\sim$15 K, validating our analysis of Fig. 1(b). The thus extracted $\gamma(n)$ are shown in Fig. 2(c), along with the calculated γ, which, for reasons clarified below, are multiplied by a

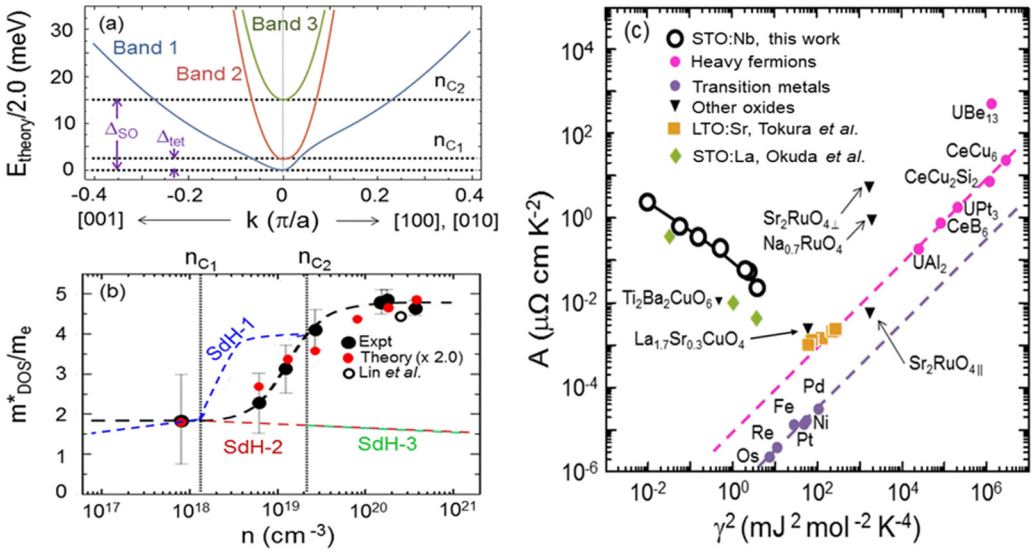

FIG. 3. (a) Band structure from a tight-binding fit to a first-principles calculation [21]. Labeled are the three bands, the tetragonality and spin-orbit splittings, and the electron densities at the Lifshitz transitions. Energies are divided by the factor 2.0. (b) Density-of-states effective mass (m^*_{DOS}/m_e) vs Hall density (n). Shown are experimental values from specific heat (black circles), theoretical values from the band structure in (a) (red circles), approximate Shubnikov–de Haas values for the three bands (blue, red, green dashed lines, measured in the cubic [100] direction [16]), and the single m^*_{DOS} from Ref. [42]. The black dashed line is a guide to the eye. (c) Kadowaki-Woods plot (A vs γ^2 on a $\log_{10}$-$\log_{10}$ plot), where A is the T^2 resistivity prefactor and γ is the Sommerfeld coefficient. Shown are Nb-doped $SrTiO_3$ (STO:Nb) results from this work (black open circles), La-doped $SrTiO_3$ (STO:La) results from Okuda *et al.* [30] (green diamonds), Sr-doped $LaTiO_3$ (LTO:Sr) results from Tokura *et al.* [52] (orange squares), along with data on various transition metals, heavy fermion compounds, and oxides from [51]. Dashed lines are linear fits; the solid line is a guide to the eye.

factor of 2.0. These values match well with the experimental data.

More detailed analysis is provided in Fig. 3(b), which plots $m^*_{DOS}(n)$ (solid black points) extracted from $\gamma(n) = m^*_{DOS}(n)n^{1/3}(k_B/\hbar)^2(\pi/3)^{2/3}$, using the measured Hall densities. We find $m^*_{DOS} \approx 1.8m_e$ below n_{c1}, increasing to $\sim 4m_e$ at n_{c2}, before plateauing at 4.5–5m_e. Note that the systematics are greatly improved over prior results from $C_P(T)$, the data also extending to lower n (see the Supplemental Material, Sec. A [35]). Quantitative consistency with SdH measurements can, in fact, be demonstrated. To this end, the blue, red, and green dashed lines in Fig. 3(b) approximate the SdH-determined m^* in the first, second, and third bands in Fig. 3(a) [16]. Starting at $n < n_{c1}$, where only one band is occupied, we find good agreement between m^*_{DOS} from C_P and m^* from SdH. For $n_{c1} < n < n_{c2}$, the SdH m^* in band 2 then stays constant, while the m^* in band 1 increases sharply, as expected from Fig. 3(a). Importantly, m^*_{DOS} reflects a weighted sum of these SdH masses. Specifically, since $\gamma(n) \propto n^{1/3}m^*$, we write (see the Supplemental Material, Sec. C [35] for justification) $m^*_{DOS} = \sum_{i=1}^{3} n_i^{1/3}m_i^* / (\sum_{i=1}^{3} n_i)^{1/3}$, where the m_i^* and n_i are SdH masses and electron densities. SdH data then predict m^*_{DOS} should increase to $4.9m_e$ at n_{c2}, in reasonable agreement with our extracted m^*_{DOS}. Finally, at $n > n_{c2}$, SdH results become sparse, especially for band 1. m^* values for bands 2 and 3 are available at 1.5×10^{20} cm^{-3}, however [16], and can be supplemented with a measurement of the ARPES heavy band mass of $7m_e$ [19] to predict $m^*_{DOS} = 5.2m_e$. This is again in good agreement with our m^*_{DOS}, as well as a single m^*_{DOS} point from the work of Lin *et al.* [42]. We thus conclude *quantitative* agreement between SdH measurements and electronic contributions to $C_P(T)$ for the filling-dependent m^* in $SrTiO_3$.

Also plotted in Fig. 3(b) (red circles) are theoretical $m^*_{DOS}(n)$ values from the tight-binding modeling shown in Fig. 3(a). Remarkably, excellent agreement with experiment is obtained simply by multiplying by a constant factor of 2.0. A mass enhancement factor of ~ 2 in $SrTiO_3$ has been deduced before at certain n [18,21], but is shown here to be completely n independent [see, also, Fig. 2(c)]. In addition to agreement with SdH measurements, we thus conclude quantitative reconciliation with the calculated band structure, with a mass enhancement factor of 2.0. As in prior work, we attribute the modest mass enhancement to effects such as electron-phonon interaction [18,21] or electronic correlations. Whatever the origin is, it is apparently unaffected by doping in the range studied here. Significantly, n-independent electron-phonon mass enhancement would also suggest that the $SrTiO_3$ superconducting dome is not caused by variations in pairing interaction.

Finally, with Fermi-liquid-like electronic C_P established, and a detailed wide-range $\gamma(n)$ available, we turn to Kadowaki-Woods scaling. Earlier $\rho(T)$ measurements were supplemented with additional data and tested for T^2 behavior. As shown in the Supplemental Material, Sec. D [35] (Figs. S2 and S3), $\rho \propto \rho_0 + AT^2$ indeed holds to reasonable confidence below 50–110 K (dependent on n), albeit with some deviations at the lowest T. As shown in Fig. S3, T^2 evolves toward T^3 at higher T [50], before the exponent falls again. Figure S4 shows that the extracted A are in good agreement with prior

work [21,30–34], following $A \propto 1/n$ over four orders of magnitude in n. Kadowaki-Woods scaling is then tested in Fig. 3(c), which plots A vs γ^2 (on a $\log_{10}$-$\log_{10}$ plot), with n as an implicit variable. The empirical $A/\gamma^2 = C$ behavior (where C is a materials-class-specific positive constant) [43,44], shown in Fig. 3(c) for transition metals and heavy fermion compounds (dashed lines), is seen to be *qualitatively* violated in doped $SrTiO_3$. Specifically, our data on $SrTiO_3$:Nb (large black circles) reveal anomalously large A at low γ, *decreasing* by a factor of 100 as γ^2 increases by a factor of 400. This trend is qualitatively consistent with the data of Okuda *et al.* [30] on $SrTiO_3$:La (green diamonds), although that data set is sparser, and, as already noted (Supplemental Material Sec. A, Fig. S1 [35]), differs significantly in terms of the values of γ, and thus m^*. Intriguingly, the decrease in A with γ in doped $SrTiO_3$ reverts to the typical Kadowaki-Woods scaling in Sr-doped $LaTiO_3$, i.e., at the La-rich end of the $Sr_{1-x}La_xTiO_3$ series (orange squares) [51]. Kadowaki-Woods scaling is thus obeyed as the Mott insulator $LaTiO_3$ is hole doped, where electronic correlations are strong, but is qualitatively violated at lower x.

A number of approaches have been explored in the literature to account for charge carrier density effects in the Kadowaki-Woods ratio (e.g., Refs. [52,53]), and we thus attempted to implement those for $SrTiO_3$:Nb. As shown in Fig. S5 (Supplemental Material, Sec. E [35]), the modified Kadowaki-Woods scaling of Jacko *et al.* [52], designed to account for doping and dimensionality effects, is also violated in doped $SrTiO_3$. We note, however, that the approach of Hussey [53] to account for doping effects in $SrTiO_3$ is successful, both for prior data in the $Sr_{1-x}La_xTiO_3$ system [53] and the current data on $SrTiO_3$:Nb (see Fig. S6, Supplemental Material, Sec. E [35]). Nevertheless, despite clear Fermi-liquid-like behavior in electronic C_P, and simply rationalized behavior of $\gamma(n)$, the doping-dependent T^2 resistivity prefactor in $SrTiO_3$ appears to differ substantially from simple Fermi liquid expectations. As noted above, it is, in fact, not even clear why T^2 resistivity occurs when umklapp processes appear impossible. This adherence to Fermi liquid behavior for thermodynamic properties, but clear deviation for transport, suggests a potentially atypical origin of the T^2 resistivity. Additional theoretical work is clearly needed, including exploring potential explanations beyond electron-electron interactions.

In summary, $C_P(T)$ measurements on single crystal $SrTiO_3$ have been performed over a wide doping range. We conclude the following: (i) lattice dynamic contributions can be understood, albeit with unusual doping sensitivity, likely related to doping evolution of soft modes; (ii) the extracted m^*_{DOS} can be quantitatively reconciled with SdH measurements and calculated band structure, yielding an n-independent mass enhancement factor of 2.0; and (iii) standard Kadowaki-Woods scaling is dramatically violated, despite the Fermi-liquid-like electronic specific heat. These results have deep implications for the origin of the puzzling T^2 resistivity in $SrTiO_3$.

This work was supported by the U.S. Department of Energy through the University of Minnesota Center for Quantum Materials under Grant No. DE-SC-0016371. E.M. thanks the Fonds de Recherche du Québec, Nature et Technologies, and the Natural Science and Engineering Research Council of Canada for fellowship support.

[1] J. H. Barrett, Phys. Rev. **86**, 118 (1952).
[2] P. A. Fleury and J. M. Worlock, Phys. Rev. **174**, 613 (1968).
[3] H. Uwe and T. Sakudo, Phys. Rev. B. **13**, 271 (1976).
[4] K. A. Muller and H. Burkard, Phys. Rev. B. **19**, 3593 (1979).
[5] J. F. Scott, Rev. Mod. Phys. **46**, 83 (1974).
[6] G. Shirane, Rev. Mod. Phys. **46**, 437 (1974).
[7] F. W. Lytle, J. Appl. Phys. **35**, 2212 (1964).
[8] P. A. Fleury, J. F. Scott, and J. M. Worlock, Phys. Rev. Lett. **21**, 16 (1968)
[9] E. McCalla, J. Walter, and C. Leighton, Chem. Mater. **28**, 7973 (2016).
[10] H. P. R. Frederikse, W. R. Thurber, and W. R. Hosler, Phys. Rev. **134**, A442 (1964).
[11] C. S. Koonce, M. L. Cohen, J. F. Schooley, W. R. Hosler, and E. R. Pfeiffer, Phys. Rev. **163**, 380 (1967).
[12] O. N. Tufte and P. W. Chapman, Phys. Rev. **155**, 796 (1967).
[13] C. Lee, J. Yahia, and J. L. Brebner, Phys. Rev. B **3**, 2525 (1971).
[14] A. Spinelli, M. A. Torija, C. Liu, C. Jan, and C. Leighton, Phys. Rev. B. **81**, 155110 (2010).
[15] C. Collignon, X. Lin, C. W. Rischau, B. Fauque, and K. Behnia, Annu. Rev. Condens. Matter Phys. **10**, 25 (2019).
[16] X. Lin, G. Bridoux, A. Gourgout, G. Seyfarth, S. Kramer, M. Nardone, B. Fauque, and K. Behnia, Phys. Rev. Lett. **112**, 207002 (2014).
[17] H. Uwe, R. Yoshizaki, T. Sakudo, A. Izumi, and T. Uzumaki, Jpn. J. Appl. Phys. **24**, 335 (1985).
[18] S. J. Allen, B. Jalan, S. B. Lee, D. G. Ouellette, G. Khalsa, J. Jaroszynski, S. Stemmer, and A. H. MacDonald, Phys. Rev. B **88**, 045114 (2013).
[19] Y. J. Chang, A. Bostwick, Y. S. Kim, K. Horn, and E. Rotenberg, Phys. Rev. B. **81**, 235109 (2010).
[20] L. F. Mattheiss, Phys. Rev. B. **6**, 4740 (1972).
[21] D. van der Marel, J. L. M. van Mechelen, and I. I. Mazin, Phys. Rev. B. **84**, 205111 (2011).
[22] A. Janotti, D. Steiauf, and C. G. Van de Walle, Phys. Rev. B. **84**, 201304 (2011).
[23] J. F. Schooley, W. R. Hosier, E. Ambler, J. G. Becker, M. L. Cohen, and C. S. Koonce, Phys. Rev. Lett. **14**, 305 (1965).
[24] X. Lin, Z. Zhu, B. Fauque, and K. Behnia, Phys. Rev. X **3**, 021002 (2013).
[25] L. P. Gor'kov, Proc. Natl. Acad. Sci. **113**, 4646 (2016).
[26] J. M. Edge, Y. Kedem, U. Aschauer, N. A. Spaldin, and A. V. Balatsky, Phys. Rev. Lett. **115**, 247002 (2015).
[27] J. Ruhman and P. A. Lee, Phys. Rev. B **94**, 224515 (2016).
[28] S. E. Rowley, C. Enderlein, J. Ferreira de Oliveira, D. A. Tompsett, E. Baggio Saitovitch, S. S. Saxena, and G. G. Lonzarich, arXiv:1801.08121.
[29] T. V. Trevisan, M. Schütt, and R. M. Fernandes, Phys. Rev. Lett. **121**, 127002 (2018).
[30] T. Okuda, K. Nakanishi, S. Miyasaka, and Y. Tokura, Phys. Rev. B **63**, 113104 (2001).
[31] J. Fukuyado, K. Narikiyo, M. Akaki, H. Kuwahara, and T. Okuda, Phys. Rev. B. **85**, 075112 (2012).

[32] X. Lin, B. Fauque, and K. Behnia, Science **349**, 945 (2015).
[33] E. Mikheev, S. Raghavan, J. Y. Zhang, P. B. Marshall, A. P. Kajdos, L. Balents, and S. Stemmer, Sci. Rep. **6**, 20865 (2016).
[34] S. Stemmer and S. J. Allen, Rep. Prog. Phys. **81**, 062502 (2018).
[35] See Supplemental Material at http://link.aps.org/supplemental/10.1103/PhysRevMaterials.3.022001 for additional information on prior literature heat-capacity parameters; materials and methods; comparison of effective masses from heat capacity, SdH, and ARPES; T^2 resistivity analysis; and Kadowaki-Woods scaling.
[36] E. Ambler, J. H. Colwell, W. R. Hosler, and J. F. Schooley, Phys. Rev. **148**, 280 (1966).
[37] J. H. Colwell, Phys. Lett. **25A**, 623 (1967).
[38] N. E. Phillips, B. B. Triplett, R. D. Clear, H. E. Simon, J. K. Hulm, C. K. Jones, and R. Mazelsky, Physica **55**, 571 (1971).
[39] I. Henning and E. Hegenbarth, Phys. Stat. Sol. (a) **83**, K23 (1984).
[40] M. Ahrens, R. Merkle, B. Rahmati, and J. Maier, Physica B **393**, 239 (2007).
[41] A. Duran, F. Morales, L. Fuentes, and J. M. Siqueiros, J. Phys.: Condens. Matter **20**, 085219 (2008).
[42] X. Lin, A. Gourgout, G. Bridoux, F. Jomard, A. Pourret, B. Fauque, D. Aoki, and K. Behnia, Phys. Rev. B **90**, 140508(R) (2014).
[43] M. J. Rice, Phys. Rev. Lett. **20**, 1439 (1968).
[44] K. Kadowaki and S. B. Woods, Sol. Stat. Commun. **58**, 507 (1986).
[45] W. D. Rice, P. Ambwani, M. Bombeck, J. D. Thompson, G. Haugstad, C. Leighton, and S. A. Crooker, Nat. Mater. **13**, 481 (2014).
[46] J. C. Lashley, M. F. Hundley, A. Migliori, J. L. Sarrao, P. G. Pagliuso, T. W. Darling, M. Jaime, J. C. Cooley, W. L. Hults, L. Morales, D. J. Thoma, J. L. Smith, J. Boerio-Goates, B. F. Woodfield, G. R. Stewart, R. A. Fisher, and N. E. Phillips, Cryogenics **43**, 369 (2003).
[47] C. W. Rischau, X. Lin, C. P. Grams, D. Fick, S. Harms, J. Engelmayer, T. Lorenz, Y. Gallais, B. Fauque, J. Hemberger, and K. Behnia, Nat. Phys. **13**, 643 (2017).
[48] E. S. R. Gopal, *Specific Heats at Low Temperatures* (Plenum, New York, 1966).
[49] N. Choudhury, E. J. Walter, A. I. Kolesnikov, and C.-K. Loong, Phys. Rev. B. **77**, 134111 (2008).
[50] X. Lin, C. W. Rischau, L. Buchauer, A. Jaoui, B. Fauque, and K. Behnia, npj Quantum Mater. **2**, 41 (2017).
[51] Y. Tokura, Y. Taguchi, Y. Okada, Y. Fujishima, T. Arima, K. Kumagai, and Y. Iye, Phys. Rev. Lett. **70**, 2126 (1993).
[52] A. C. Jacko, J. O. Fjaerestad, and B. J. Powell, Nat. Phys. **5**, 422 (2009).
[53] N. E. Hussey, J. Phys. Soc. Jpn. **74**, 1107 (2005).